Astron. Astrophys. 54, 61 – 70 (1977)

ASTRONOMY AND ASTROPHYSICS

Acoustic Waves in the Solar Atmosphere I, The Hydrodynamic Code

P. Ulmschneider[1], W. Kalkofen[2], T. Nowak[1] and U. Bohn[1]

[1] Institut für Astrophysik, D-8700 Würzburg, Federal Republic of Germany
[2] Center for Astrophysics, Cambridge, Mass. 02138, USA

Received February 20, revised July 19, 1976

Summary. This is the first in a series of papers studying large amplitude, radiatively damped acoustic waves in the solar atmosphere. We describe a modified method of characteristics for the solution of the time-dependent hydrodynamic equations in a gravitational atmosphere. A new procedure for the detection of shocks is outlined. Several tests of the accuracy of the method are described. We have computed the evolution of the wave and the height of shock formation for several values of the period and the initial acoustic flux, in isothermal atmospheres with temperatures 4000 and 5000 K, and in a model solar atmosphere.

Key words: acoustic waves — shocks — radiation damping — chromosphere

I. Introduction

Biermann (1946) and Schwarzschild (1948) were the first to suggest that the solar chromosphere and corona are heated by the dissipation of shock waves developing from acoustic waves generated in the turbulent field of the convection zone. A test of this acoustic heating theory was difficult because of both observational and mathematical problems.

On the theoretical side, the computation of acoustic waves has two main sources of difficulties. One is the nonlinear nature of the hydrodynamic equations, which allows the development of a sinusoidal acoustic wave into a sawtooth-type shock wave. Here the problem is mainly associated with the mathematical formalism of treating this nonlinearity accurately, i.e., to follow the distortion of the wave to the point of shock formation and to compute the wave in the presence of shocks. The other difficulty is due to the importance of radiative damping, which severely decreases the mechanical energy of the waves. This transformation of mechanical energy into optical radiation depends on the acoustic wavelength and on the optical depth. It is especially severe in the range of

$$0.1 \leqq \tau_{5000} \leqq 10 .$$

For earlier work in the field of radiation hydrodynamics, we refer to the books by Pai (1966) and Vincenti and Krüger (1965). However, these books and the literature cited therein do not treat the radiation losses adequately for our purposes. The optically thin or diffusion approximations usually employed are valid for small or very large optical depths, respectively, but break down in the region near $\tau_{5000}=1$, where the dominant radiation loss occurs. Only very recently have the hydrodynamic equations been solved with the simultaneous solution of the transfer equation of radiation (Klein, 1973; Cannon, 1974; Klein et al., 1976; Kneer and Nakagawa, 1976). These authors have treated the radiation damping with differential equation methods and, in addition, have allowed simultaneously for departures from local thermodynamic equilibrium (LTE).

In this first (Paper I) of a series of papers, we describe the hydrodynamic code and show how the radiative losses are treated in the equations. In the second (Paper II, Kalkofen and Ulmschneider, 1976) an integral method is developed to treat the radiative damping. The third paper (Paper III, Ulmschneider and Kalkofen, 1976) shows how the acoustic heating theory can be used to predict the location of the temperature minimum in the Sun. Here we show the basic equations in the Lagrange representation. We then give the reasons for our selection of the characteristics method to solve the equations and discuss the initial conditions and the choice of space and time steps. The numerical treatment is described along with the interpolation and extrapolation procedures and the method used to find the point where a shock forms. We conclude by discussing several tests of the accuracy of our solution and present the result of adiabatic calculations for waves in solar atmosphere models.

Send offprint requests to: P. Ulmschneider

II. Basic Equations

The hydrodynamic equations describing acoustic waves in a gravitational atmosphere are given by Landau and Lifshitz (1959, pp. 2, 4, 49, 185). For applications to the solar atmosphere these equations must be augmented by the equations of radiative transfer (see Paper II) because of the low value of the Boltzmann number, the ratio of convective to radiative fluxes. The appearance of shocks in the continuous flow complicates these equations, as does the influence of ionization and of departures from local thermodynamic equilibrium, LTE (discussed in Paper II). In view of the great complexity and long computation time of a completely general treatment we have made a number of simplifying assumptions in order to make the problem tractable. Furthermore, we have restricted the region of applicability of our calculations to the photosphere and low chromosphere, for which we use the HSRA model (Gingerich et al., 1971). First, we assume that the acoustic waves propagate only in the vertical direction. Second, an evaluation of the mean molecular weight μ and of the ratio γ of specific heats in the HSRA shows that for the upper photosphere and the low chromosphere we may take μ and γ to be constant. The values we use are $\mu=1.3$ g/mol and $\gamma=5/3$. These assumptions still hold if acoustic waves are present because the Mach numbers (in the Euler frame) of the waves are small, typically between $M=0.03$ in the photosphere and $M=0.3$ in the chromosphere. Other effects of ionization are neglected as well, except for the influence on opacity.

Third we neglect the details of the hydrodynamic shock structure and treat it as a discontinuity. Thus the detailed dependence of the thermodynamic variables and the flow velocity on height are misrepresented over a distance of a few atomic mean free paths. The atomic mean free path however is only about 0.01 cm in the photosphere and about 1 cm in the low chromosphere. This is very small compared to both the wavelength and the scale-height. Contrary to the situation for strongly ionizing shock waves of large Mach number (Cannon, 1974), the optical depth over a mean free path in our case of small amplitude waves is only about $\Delta\tau=1$ E–10. Thus radiation is unimportant for the structure of the hydrodynamic shock and hence the radiative flux may be neglected in the Hugoniot relations. Since the entropy increase is independent of the detailed dissipation mechanism (Zeldovich and Raizer, 1967, p. 471) and since it is correctly predicted by the Hugoniot relations, the treatment of the shock as a discontinuity will be a very good approximation. Note, that in many applications, as for example to strong shocks in variable stars (e.g. Castor, 1972), not only the hydrodynamic shock but also the adjoining radiative relaxation regions are included under the term shock. We do not follow this usage but rather take shock to mean only the hydrodynamic discontinuity. The pre- and post shock radiative relaxation regions are treated explicitly in our work.

Fourth, viscous and thermal conduction effects are neglected in the non shock regions. This may be justified taking viscosity and thermal conductivity coefficients from Brezing (1965) and Ulmschneider (1970) and assuming a typical wave period of 30 s (Stein, 1968) and a typical velocity amplitude of $u=c/10$, where c is the sound velocity.

For mathematical convenience we use the Lagrange frame, where the Lagrange coordinate a is the geometrical coordinate of a gas particle at time $t=0$ (Courant and Friedrichs, 1948, p. 13). The Euler coordinate x is given by

$$x=x(a,t)\,, \tag{1}$$

the flow velocity u by

$$u=\left(\frac{\partial x}{\partial t}\right)_a\,. \tag{2}$$

Conservation of mass is described by the two equations

$$v\equiv\left(\frac{\partial x}{\partial a}\right)_t=\frac{\varrho_0}{\varrho}\,, \tag{3}$$

and

$$\left(\frac{\partial \varrho}{\partial t}\right)_a+\frac{\varrho}{v}\left(\frac{\partial u}{\partial a}\right)_t=0\,, \tag{4}$$

where $\varrho(a,t)$ and $\varrho_0(a)$ are the density distributions at times t and $t=0$ and v is the dimensionless specific volume. The equation of motion reads

$$\left(\frac{\partial u}{\partial t}\right)_a+\frac{1}{\varrho_0}\left(\frac{\partial p}{\partial a}\right)_t+g=0\,. \tag{5}$$

Here p is the gas pressure and $g=2.736$ E4 cm/s^2 is the solar gravitational acceleration. The energy equation is given by

$$\left(\frac{\partial S}{\partial t}\right)_a=\left.\frac{dS}{dt}\right|_{\mathrm{Rad}}\,, \tag{6}$$

where S is the entropy and $\left.\frac{dS}{dt}\right|_{\mathrm{Rad}}$ is the radiative damping function, which is assumed to be given as a function of ϱ, T, and a (see Paper II). The combined first and second law of thermodynamics connects S with ϱ and temperature T:

$$TdS=c_v dT+pd\left(\frac{1}{\varrho}\right), \tag{7}$$

where for constant γ the specific heat c_v is given by

$$c_v=\frac{1}{\gamma-1}\frac{R}{\mu}\,, \tag{8}$$

and where $R=8.3144$ E7 erg/mol K is the universal gas constant. In Equation (7) we have neglected the absorption of energy due to H ionization. This energy

becomes important in the high chromosphere. With the equation of state for an ideal gas,

$$p=\varrho\frac{RT}{\mu}, \tag{9}$$

the problem is now posed by the six Equations (3) to (7) and (9), which are to be solved for the six unknowns, u, ϱ, p, T, v and S.

III. Method of Characteristics

Several recent workers (Leibacher, 1971; Stein and Schwarz, 1972, 1973; Klein, 1973; Cannon, 1974; Klein et al., 1976; Kneer and Nakagawa, 1976) have chosen the finite difference method for solving the posed system of partial differential equations [Eqs. (3) to (6)]. Apart from the different treatments of radiation (discussed in Paper II) the handling of the shock among these workers differs greatly. The most detailed calculation was done by Cannon (1974) who computed the shock structure. Replacement of the shock by a discontinuity as in our characteristics method represents a less detailed treatment over a distance that is of the order of a few mean free paths. However as discussed previously, the errors in this approximation are quite small because first the thickness of the shock is very small compared to characteristic length scales of our problem and second because due to the small optical thickness across the shock, the entropy jump is given correctly by the radiationless Hugoniot relations, regardless of the detailed shock structure. Thus the replacement of the shock by a discontinuity does not result in significant loss of accuracy in this case. Loss of accuracy can occur, however, if the shock is computed with the artificial viscosity method. There the hydrodynamic variables and the source function of radiation are changed significantly over several macroscopic grid points. This led us to adopt the characteristics method which, in addition, needs fewer points to represent a wave and allows faster advance in time.

The method of characteristics that we employ is the constant time step version due to Hartree (1952), described by Lister (1960), Hoskin (1964) and Stefanik (1973). We eliminate all thermodynamic variables except two, for which we choose the entropy S and the sound velocity c, which in the regions where H ionization is neglected, may be defined by

$$c^2=\gamma\frac{RT}{\mu}. \tag{10}$$

To eliminate p and ϱ from the equations we find from Equations (7), (9) and (10)

$$dp=\frac{2c}{\gamma-1}\varrho dc-\frac{\mu c^2}{\gamma R}\varrho dS \tag{11}$$

and

$$d\varrho=\frac{2}{\gamma-1}\frac{\varrho}{c}dc-\frac{\mu\varrho}{R}dS. \tag{12}$$

Eliminating derivatives of p and ϱ from Equations (4) and (5), we have

$$\frac{2}{\gamma-1}\frac{\partial c}{\partial t}-\frac{\mu c}{R}\frac{\partial S}{\partial t}+\frac{c}{v}\frac{\partial u}{\partial a}=0 \tag{13}$$

and

$$\frac{\partial u}{\partial t}+\frac{2}{\gamma-1}\frac{c}{v}\frac{\partial c}{\partial a}-\frac{\mu c}{\gamma R}\frac{c}{v}\frac{\partial S}{\partial a}+g=0. \tag{14}$$

If we add Equation (13) to (14) and use (6), the ordinary differential equation,

$$du+\frac{2}{\gamma-1}dc-\frac{\mu c}{\gamma R}\left(dS+(\gamma-1)\frac{dS}{dt}\bigg|_{\text{Rad}}dt\right)+gdt=0, \tag{15}$$

is obtained along the C^+ characteristic, which is given by the equation

$$\frac{da}{dt}=\frac{c}{v}. \tag{16}$$

Similarly we get the differential equation,

$$du-\frac{2}{\gamma-1}dc+\frac{\mu c}{\gamma R}\left(dS+(\gamma-1)\frac{dS}{dt}\bigg|_{\text{Rad}}dt\right)+gdt=0, \tag{17}$$

along the C^- characteristic, given by

$$\frac{da}{dt}=-\frac{c}{v}. \tag{18}$$

Finally from Equation (6), we have

$$dS=\frac{dS}{dt}\bigg|_{\text{Rad}}dt \tag{19}$$

along the C^0 characteristics, $a=\text{const}$.

From Equations (3), (12), (16) and (18) and with $\gamma=5/3$, we obtain the specific volume,

$$v=\left(\frac{\partial x}{\partial a}\right)_t=\left(\frac{c_0}{c}\right)^3 e^{-\frac{(S-S_0)\mu}{R}}, \tag{20}$$

where c_0 and S_0 are the sound velocity and the entropy distribution in the undisturbed atmosphere.

IV. Initial State and Grid Selection

With a given arbitrary temperature distribution, hydrostatic equilibrium is enforced when the initial sound velocity c_0 is computed from Equation (10) and the initial entropy distribution S_0 is determined from Equation (14):

$$\frac{dS_0}{da}=\frac{\gamma R_0}{\mu c_0}\left(\frac{2}{\gamma-1}\frac{dc_0}{da}+\frac{g}{c_0}\right). \tag{21}$$

The choice of the height grid is limited by two height scales: A sinusoidal wave should be represented by at least ten points per wavelength, and there should be at

least ten points per scale height. Thus we have chosen a height step Δa such that

$$\Delta a = \mathrm{Min}\left(\frac{\lambda}{10}, \frac{H}{10}\right), \tag{22}$$

where λ is the wavelength and

$$H = \frac{RT}{\mu g} \tag{23}$$

the scale height.

The time step Δt in Hartree's (1952) method is chosen to be

$$\Delta t = 0.9 \frac{\Delta a}{c_0} \tag{24}$$

in order to exclude extrapolations and to include only neighboring points for interpolation. In principle, however, we are not bound to the Courant condition because the method of characteristics automatically ensures that the points at the new time stay within the domain of dependence. In an isothermal atmosphere, e.g., the numerical factor in Equation (24) may be chosen equal to unity to simulate a moving boundary condition.

V. Numerical Treatment

The detailed numerical treatment proceeds as shown by Lister (1960) and Hoskin (1964) and will not be repeated here.

V.1. Method of Solution

We assume that at the old time the solution is given at grid points and at a number of special points like boundary or shock points. Because radiation transport occurs essentially instantaneously (see Paper II) the full characteristics method, where the solution advances with unequal time steps, cannot be applied. Instead we use the modified characteristics method due to Hartree (1952) which allows for a constant time step Δt. Thus the position of the grid at the new time $t+\Delta t$ is known. For radiation (see Paper II) we assume the radiative damping function

$$D \equiv \left.\frac{dS}{dt}\right|_{\mathrm{Rad}} \tag{25}$$

to be given at every grid and special point in the old as well as the new time level. For adiabatic cases D is zero. The entropy S at the points of the new time level is computed by integrating Equation (19) along the C^0 characteristic using the trapezoidal rule. The remaining unknowns, u and c, are then found by integrating Equations (15) and (17), respectively, along the C^+ and C^- characteristics given by Equations (16) and (18). Since the slopes of the C^+ and C^- characteristics are known only at the old time level an iterative procedure is necessary. We found that about four iterations were needed for a relative error of 1.0 E-8 in u or c.

For non interior points the treatment is slightly modified. At the lower boundary the velocity is known from the prescribed piston motion and only c needs to be iterated along the C^- characteristics. For the piston velocity we usually took

$$u = -u_0 \sin\left(\frac{2\pi}{P} t\right), \tag{26}$$

where u_0 is given by Equation (38) and P is the period at the acoustic wave. At the upper boundary we usually took a "transmitting" boundary condition as used by Leibacher (1971) and Stein (1972). Here the velocity amplitude u is assumed constant along the C^+ characteristic. This choice is suggested by comparison to sound and simple waves, where the constancy of u is rigorously true. The constancy of u is however only approximately true in more general situations. In our cases the transmitting boundary condition was found to give excellent transmission even for waves with large amplitudes less than c.

At the shock, which is treated as a discontinuity that separates the preshock region 1 from the postshock region 2, we search for the solution at two infinitesimally separated points. As described by Hoskin (1964) there are the characteristics C^+, C^0 and C^- that emanate from the preshock point and the C^+ characteristic from the postshock point. Thus from the integration of Equations (15) to (19) we find four of the seven unknowns, u_1, c_1, S_1, u_2, c_2, S_2 and the shock velocity U_{SH}. The remaining three unknowns are determined by the three Hugoniot relations (Landau and Lifshitz, 1959, p. 319), which in cases of no ionization may be written

$$U_{SH} = u_1 + \frac{\gamma+1}{4}(u_2-u_1) + \left[\left(\frac{\gamma+1}{4}\right)^2 (u_2-u_1)^2 + c_1^2\right]^{1/2}, \tag{27}$$

$$c_2 = \left[\frac{\gamma-1}{2}(V_1^2 - V_2^2) + c_1^2\right]^{1/2}, \tag{28}$$

and

$$S_2 = S_1 + \frac{2}{\gamma-1}\frac{R}{\mu}\ln\frac{c_2}{c_1} - \frac{R}{\mu}\ln\frac{V_1}{V_2}. \tag{29}$$

where

$$V_1 \equiv u_1 - U_{SH} \tag{30}$$

and

$$V_2 \equiv u_2 - U_{SH}. \tag{31}$$

The slope of the shock path in the Lagrangian frame is given by

$$\left(\frac{\partial a}{\partial t}\right)_{SH} = (U_{SH}-u_1)\left(\frac{\partial a}{\partial x}\right)_t. \tag{32}$$

A hierarchy of iterations is employed in order to find the shock position and to integrate the unknown quantities with the trapezoidal rule. Since this procedure is strongly oscillatory, damping was introduced by averaging u_2 with the previously computed value. For grid points in the vicinity of boundaries, special treatment is necessary because of the intersection of characteristics with the boundaries. In such cases we obtained the solution at the boundary by means of an interpolation.

V.2. Interpolation and Extrapolation Procedures

The method of characteristics of Hartree (1952), in contrast to the full characteristics method, involves interpolation of solutions at the old time level. This may be performed in several ways. Hartree (1952) used parabolic interpolation and ensured that the pair of C^+ and C^- characteristics emanating from a point in the new time level always fell within $\pm\Delta a$ of the position of the point in the old time level. This forces the time step [see Eq. (24)] to be close to the Courant time. In principle one is not bound to this procedure and one can allow for time steps greater than the Courant time. However, when many grid points fall between the intersection points of the C^+, C^- pair, the accuracy is lowered since the influence of the intermediate points on the curvature of the characteristics is ignored. Thus we always kept close to the Courant condition. Other types of interpolation either lead to poor solutions, as for linear interpolation, or to long computation times, as for interpolation employing higher order polynomials.

Extrapolation to zero step size, as described by Lister (1960) and used already by Richardson and Gaunt (1927), also may lead to difficulties when used in the modified characteristics method. This method increases the accuracy considerably when applied to the full characteristics method, as shown recently by Smith (1970). For the modified characteristics method, however, we found that this procedure amplifies the errors of the parabolic interpolation scheme and leads to oscillations in the compression region, eventually resulting in double peaks. Note that this oscillation has nothing to do with oscillations appearing in the same region when using finite difference methods but is simply a result of the parabolic interpolation. This can be demonstrated by comparison with the full characteristics method where these oscillations do not occur. We found that discarding the extrapolation procedure improved the solution considerably.

V.3. Shock Finding and Insertion

In the modified method of characteristics, the shock finding procedure presents certain difficulties that are not found in the full method of characteristics. Shocks appear in a continuous flow whenever characteristics of the same family intersect. We thus followed C^+ characteristics from adjacent grid points by integrating Equation (16) with the trapezoidal rule. Here the slopes da/dt at the new time level were interpolated after the solution is known. Straight line intersection of two C^+ characteristics predicts the position and time t_{SH} of shock formation. When the characteristics were close to intersection, however, we found that if t is the time of the last computed level then shock times t_{SH} less than $t+\Delta t$ were never found, and at every time step, t_{SH} was increased by Δt. We avoided this difficulty that is due to interpolation, by always keeping only the lowest value of t_{SH}. In order to take into account the fact that the approach to the shock should involve interpolation curves of higher order than second, Stefanik (1973) employed the three left points of four grid points for the interpolation of the left C^+ characteristic. This procedure led to satisfactory shock finding.

In order to avoid following a large number of characteristics we employed a method that allows the shock to be found without integration of characteristics. Since the position where the shock might occur can be found by searching for the maximum of the slope difference

$$\Delta y_{\mathrm{Max}} \equiv \left.\frac{da}{dt}\right|_{C_1^+} - \left.\frac{da}{dt}\right|_{C_2^+} \tag{33}$$

of adjacent grid points 1 and 2 we may compute the separation ΔA of the two C^+ characteristics by using

$$\Delta A = \Delta A_{\mathrm{Old}}(\Delta a - \Delta y_{\mathrm{Max}}\Delta t)/\Delta a\,, \tag{34}$$

where ΔA_{Old} is the separation at the previous time step and originally $\Delta A_{\mathrm{Old}} = \Delta a$.

The shock is inserted whenever t_{SH} is found at a time t less than $t = t_{\mathrm{Old}} + \Delta t$. This procedure is different from that of Stefanik (1973), who inserted the shock at a much later time. At the midpoint in the interval where Δy_{Max} is found we interpolate with Stefaniks method u_1, c_1, D_1 and $S_2 = S_1$ using the three forward points, and u_2, c_2, D_2 using the three backward points. This method never led to any oscillation of the type found by Stefanik (1973) and the increase of the entropy perturbation always proceeded in a smooth monotonic manner.

VI. Tests

We have tested our numerical procedure in several ways. Direct tests were done to check the conservation of energy. Using Equations (7) to (10) we derive an energy conservation equation in the Lagrange frame,

$$\frac{\partial}{\partial t}\left(\varrho_0 c_V T + \frac{1}{2}\varrho_0 u^2\right) + \frac{\partial (up)}{\partial a} + \varrho_0 u g - \varrho_0 T \left.\frac{dS}{dt}\right|_{\mathrm{Rad}} = 0\,,$$

which is similar to an equation given by Landau and Lifshitz (1959, p. 11). Here ϱ_0 is the density of the un-

disturbed atmosphere. Integrating the five energy terms in Equation (35) individually over time and over a vertical column, one square centimeter in area extending from $a=0$ to $a=a_{\mathrm{Max}}$, we find energy conservation to be accurate to about three significant figures. Because no error accumulated in time after many time steps, we attribute the remaining error to the integration and consider the convergence of the total energy established. The Euler grid x was calculated by integrating Equation (3), evaluating the piston position directly from Equation (26).

Energy flux conservation was checked by computing the mechanical flux

$$\pi F_M = \int_{t_a}^{t} (p-p_0)u\,dt \Big/ \int_{t_a}^{t} dt \tag{36}$$

where p and p_0 are the instantaneous and the initial pressures. At frequencies high compared to the cut off frequency this flux can also be found by using

$$\pi F_M = \int_{t_a}^{t} \varrho_0 c_0 u^2\,dt \Big/ \int_{t_a}^{t} dt\cos\alpha \tag{37}$$

where α is the phase shift [cf. Eq. (52)]. Here t_a is the arrival time of the wave at the height where the flux is being computed. t_a was evaluated under the assumption that the initial disturbance, usually an expansion wave, travels with sound velocity. The flux πF_M as a function of time t oscillates with decreasing amplitude around the average flux value. This average flux is equal to πF_M at large t or simply at $t=t_a+P$. With Equation (37) we were able to check whether the initial flux πF_I introduced at the lower boundary according to Equation (26) and with

$$u_0 = \left[\frac{2\pi F_I}{\varrho_0(1)c_0(1)}\right]^{1/2}, \tag{38}$$

propagates through the atmosphere. An accuracy of a few percent was found for flux conservation in adiabatic cases.

We performed checks against analytic solutions for a number of cases. Deviations were always found to be far less than one percent when compared with simple wave solutions. Very good agreement with analytic results was also found in the case of a constant velocity piston (Landau and Lifshitz, 1959, p. 357). This solution allowed to test the jump conditions, the velocity of the shock, and the integration of the shock path through the Lagrange space. The analytic solution of the constantly accelerated piston (Courant and Friedrichs, 1948, p. 110) serves as an excellent test for our shock finding procedure. We have varied the grid size by a factor of ten and found the shock in each case within Δa and Δt of the true position. Again, in contrast to Stefanik (1973) we found that the variables behind the shock did not show oscillatory behavior.

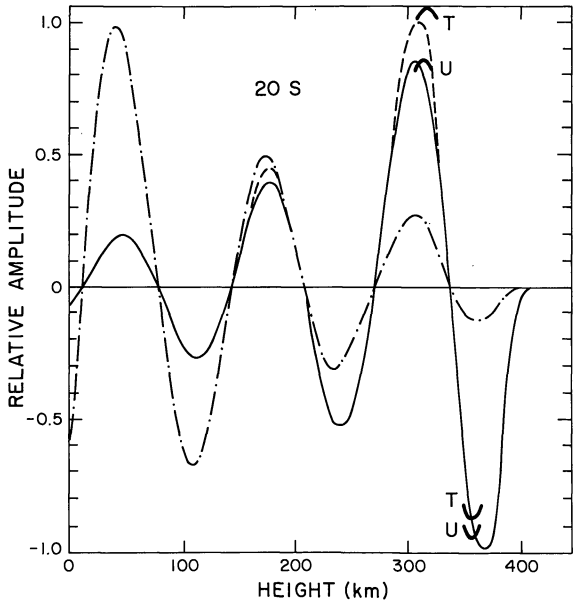

Fig. 1. Acoustic wave with a period of $P=20$ s and an initial flux of $\pi F_I=2$ E7 erg/cm^2 s at time $t=61$ s. The ordinates must be multiplied by the values in parentheses: gas velocity U (drawn) (1.60 E4 cm/s), temperature T' (dashed) (6.00 E1 K), and pressure perturbation P' (–·–) (1.32 E4 dyn/cm^2). The calculation with the flux of $\pi F_I=$ 1.6 E8 for the same time is indicated by short arcs at the maxima and minima. The ordinates for this calculation are larger by a factor of $\sqrt{8}$ than those of the low flux wave

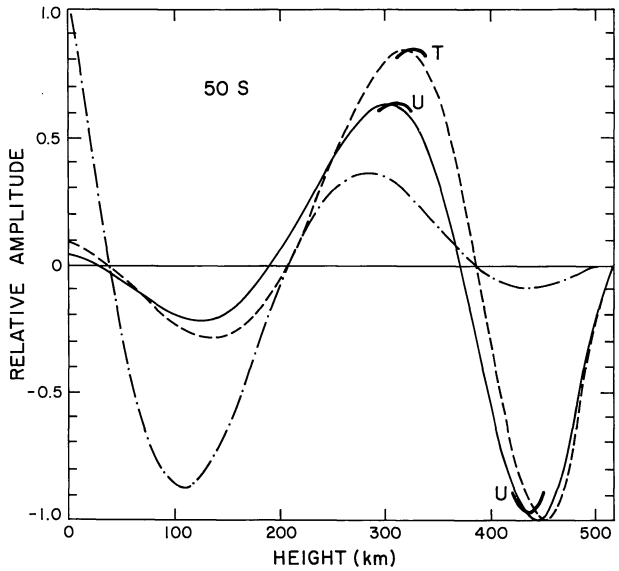

Fig. 2. Acoustic wave with a period of $P=50$ s and a flux of $\pi F_I=$ 2 E7 erg/cm^2 s at $t=78$ s, with the same symbols as those of Figure 1. For an amplitude of unity, the ordinates are $U=2.00$ E4, $T'=6.81$ E1 and $P'=1.01$ E4. For $\pi F_I=1.6$ E8 erg/cm^2 s the ordinates are scaled by $\sqrt{8}$

VII. Results

VII.1. Isothermal Gravitational Atmosphere

Figures 1 to 4 show calculations of acoustic waves in an isothermal gravitational atmosphere with a temperature

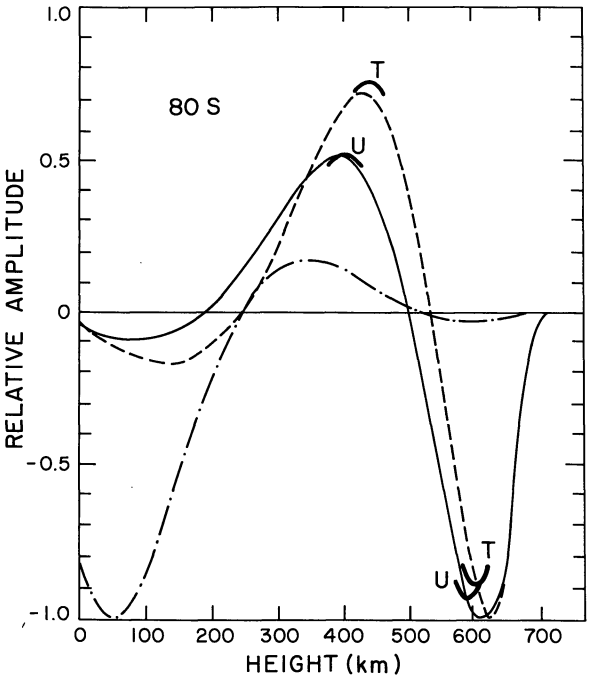

Fig. 3. Acoustic wave with a period of $P=80$ s and a flux of $\pi F_I=$ 2 E7 erg/cm^2 s at $t=10$ s. For meaning of symbols, see Figure 1. For an amplitude of unity, the ordinates are $U=3.51$ E4, $T'=1.15$ E2 and $P'=1.23$ E4. For a flux of $\pi F_I=1.6$ E8 erg/cm^2 s the ordinates are scaled by $\sqrt{8}$

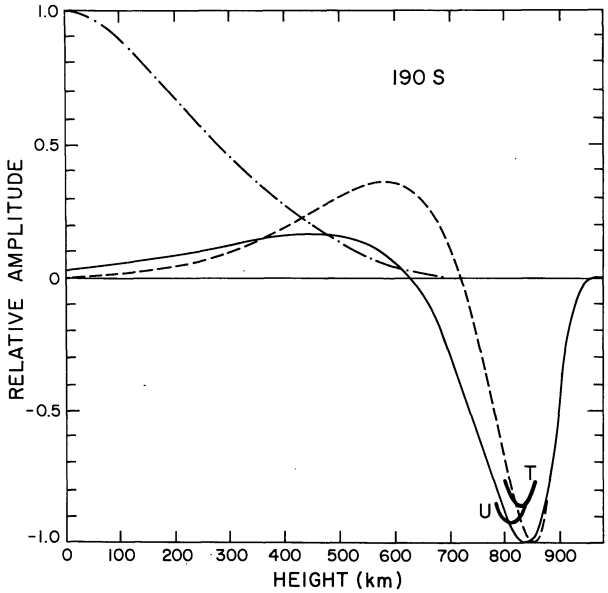

Fig. 4. Acoustic wave with a period of $P=190$ s and a flux of $\pi F_I=$ 2 E7 erg/cm^2 s at $t=143$ s. For symbols see Figure 1. The ordinates at unit amplitude are $U=5.20$ E4, $T'=1.65$ E2 and $P'=2.60$ E3. For $\pi F_I=1.6$ E8 erg/cm^2 s the ordinates are scaled by $\sqrt{8}$

$T_0=4000$ K. The gravitational acceleration has the solar value $g=2.736$ E4 cm/s^2, and the density at the lowest point is $\varrho_{00}=1.0$ E5 g/cm^3. The wave was excited by a piston oscillating sinusoidally according to Equations (26) and (38) for a chosen value of the initial flux πF_I. Figures 1 to 4 give the results for periods $P=20$, 50, 80 and 190 s with initial flux $\pi F_I=2.0$ E7 erg/cm^2 s and, indicated by short arcs, with $\pi F_I=1.6$ E8 erg/cm^2 s. Displayed in these figures are the gas velocity u, the temperature disturbance $T'=T-T_0$, and the pressure disturbance $p'=p-p_0$. In order to minimize the effects of transients, we always started with an expansion wave.

a. Comparison with Linear Theory

It is interesting to compare these results with the linear theory of small amplitude waves. Since the results of the linear theory in the Lagrange frame exhibit characteristic differences compared to the results in the Euler frame (Hines, 1960; Pitteway and Hines, 1965), we show here the relevant equations for the Lagrange frame. Taking an isothermal gravitational atmosphere with the scale height H in the Lagrange frame, we obtain from Equations (3) to (5) by linearization

$$\frac{\partial \varrho'}{\partial t}+\varrho_0\frac{\partial u}{\partial a}=0 \tag{39}$$

and

$$\frac{\partial u}{\partial t}+\frac{c_0^2}{\varrho_0}\frac{\partial \varrho'}{\partial a}=0\,, \tag{40}$$

where

$$p'=p-p_0 \tag{41}$$

and

$$\varrho'=\varrho-\varrho_0\,, \tag{42}$$

with p' and ϱ' as well as u assumed to be small. For vertical propagation of the sound wave, we assume

$$\varrho'=\varrho_0 R A e^{i(\omega t-Ka)} \tag{43}$$

and

$$u=UAe^{i(\omega t-Ka)}\,, \tag{44}$$

where

$$K=k+ib \tag{45}$$

is a complex wavenumber vector, A an arbitrary amplitude, $\omega=2\pi\nu$ the wave frequency, and R and U complex polarization factors.

We find the characteristic equation,

$$\begin{pmatrix} i\omega & -ik+b \\ -ikc_0^2+bc_0^2-\dfrac{c_0^2}{H} & i\omega \end{pmatrix}\begin{pmatrix} R \\ U \end{pmatrix}=0\,, \tag{46}$$

which has a nontrivial solution only if

$$b=\frac{\omega_1}{c_0} \tag{47}$$

and

$$\omega^2-\omega_1^2=k^2c_0^2\,, \tag{48}$$

where

$$\omega_1\equiv\frac{\gamma g}{2c_0}=\frac{c_0}{2H} \tag{49}$$

is the acoustic cut-off frequency, as in the Euler frame. However, the solution for R and U,

$$R=\left[\left(1-\left(\frac{\omega_1}{\omega}\right)^2\right)^{1/2}+i\frac{\omega_1}{\omega}\right] \tag{50}$$

and

$$U=c_0\,, \tag{51}$$

is different from that in the Euler frame. The phase shift α of the density oscillation relative to the velocity oscillation is given by

$$\alpha=\arctan\left[\frac{\omega_1/\omega}{(1-(\omega_1/\omega)^2)^{1/2}}\right]. \tag{52}$$

Since, in the adiabatic case, the entropy in a fluid element is constant, both temperature and pressure oscillations have the same phase shift as the density oscillation. This is contrary to the solution in the Euler frame, where the temperature and density oscillations are 180° out of phase for $\omega\to\omega_1$. Figures 1–4 demonstrate the behavior that is typical for the Lagrange frame, where the phase shifts of p', ϱ' and T' coincide. These values always have a common node with a forward phase shift α relative to the velocity oscillation. The phase shifts found numerically were 3.0 km for a wave with a period of $P=20$ s, 16 km for 50 s and 42 km for the 80-s wave. These values are in rough agreement with the height shifts Δh of the linear theory

$$\Delta h=c_0\frac{\alpha}{2\pi}P \tag{53}$$

for a cut-off period of $P_1=180$ s and $\omega_1=2\pi/P_1$. Equation (53) gives $\Delta h=2.3$ km for $P=20$ s, 14.6 km for 50 s and 38.3 km for 80 s. The differences between theory and numerical computation are most likely due to transients. The steepening influence of the decreasing density in the gravitational atmosphere is obvious in Figures 1–4.

For the 20-s wave, Equations (44)–(49) are satisfied to an accuracy of about 1%, as judged by the ratio of successive maxima and minima. For the 50-s wave, the accuracy is still 8%. As in the case of phase shifts, it is again obvious that for longer periods the effect of transients is more pronounced; it can easily be seen in Figure 4 where the height difference between the head of the wave and the first node is much smaller than the value of $\lambda/2=620$ km of a 190-s wave. This wave, which has a longer period than the cut-off period of $P_1=180$ s, transmits much energy but will eventually be strongly damped, as is predicted by the linear theory.

In computations for the same periods but the larger flux of $\pi F_I=1.6$ E8 erg/cm^2 s, we note the familiar scaling law for sound waves. We have indicated the results of these calculations by short arcs near the maxima and minima of the low flux values. In sound waves, the amplitude is proportional to the square root of the flux. As can be seen in Figures 1–4, the results for the flux of 1.6 E8 erg/cm^2 s, scaled by $\sqrt{8}$, are almost the same as those for the flux of 2.0 E7 erg/cm^2 s. Thus, the scaling law appears to be valid over a large range of initial fluxes. For an acoustic flux smaller than about 1.6 E8 erg/cm^2 s, the solution may be obtained from Figures 1–4 by scaling.

b. Heights of Shock Formation

Figure 5 shows the heights of shock formation in isothermal gravitational atmospheres with temperatures of $T_0=4000$ and 5000 K and the solar gravity of $g=2.736$ E4 cm/s^2. The values labeling the curves represent the initial fluxes πF_I that were used in Equation (38) in order to compute the velocity amplitude of the piston. For small periods ($\leqq 80$ s), this flux represents $\cos\alpha$ times the actual acoustic flux. It is seen that the shock heights increase with period. This well known effect (see, e.g., Ulmschneider, 1971a) can be understood from the theory of simple waves. We have compared these

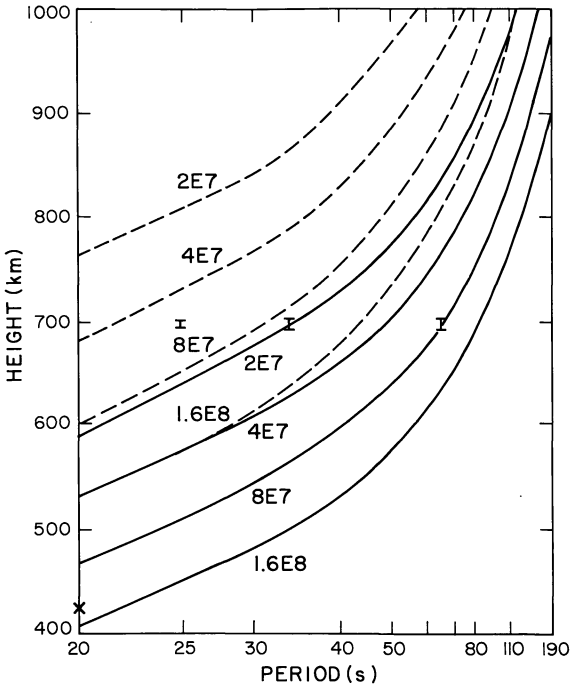

Fig. 5. Height (Eulerian) of shock formation versus period of acoustic waves in isothermal gravitational atmospheres with temperatures of 4000 K (drawn) and 5000 K (dashed) and initial flux πF_I in (erg/cm^2 s) as parameter. Error bars indicate grid size Δa. X marks the calculation for $\pi F_I=1.6$ E8 erg/cm^2 s with $2\Delta a$

heights with formula (6) of Stein and Schwartz (1972) using $\lambda = c_0 P/2$ and u_0 from Equation (38). We found some discrepancies, suggesting that Stein and Schwartz's equation overestimates the shock heights by about 10–20% (see Table 1). From Figure 5 it is seen that a factor-of-two increase in flux decreases the shock height by a constant difference of about 60 km. This height difference was also found from Stein and Schwartz's formula, which suggests that their formula needs to be corrected by subtracting about 50 km, or half a scale height.

In Figure 5, we show the influence of the grid size on our calculations. We always used about 28 points per wavelength [cf. Eq. (27)] and ensured that $\Delta a < H/14$. The grid size is indicated by error bars in Figure 5. By reducing the stepsize to $\Delta a/2$ we found the same shock heights within $\Delta a/2$. Only when we doubled the stepsize to $2\Delta a$ were somewhat larger shock heights obtained, as indicated for one case in Figure 5. Even in this case of 14 points per wavelength, the shock heights were found to within $4\Delta a$ of the true location. This behavior demonstrates the advantage of the characteristics method over the finite difference method because the former needs only a very small number of points per wavelength.

c. Shock Propagation

The formation of the shock and the computation of the shock propagation are shown in Figure 6 for a wave with a period $P = 80$ s and an initial flux of $\pi F_I = 8$ E7 erg/cm^2 s at time $t = 164$ s. We see that the entropy perturbation $S' = S - S_0$ representing the shock dissipation increases rapidly. The shock has attained a sawtooth profile and has reduced the width of the expansion region in front. A comparison of the dissipation with the results of the weak shock theory is planned for a separate work.

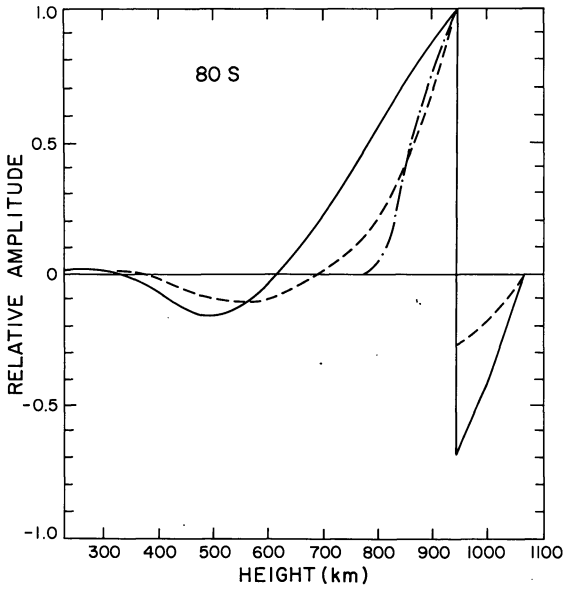

Fig. 6. Acoustic wave with a period of $P = 80$ s and a flux of $\pi F_I = 8$ E7 erg/cm^2 s at $t = 164$ s. For legend see Figure 1. Insertion and growth of the shock are shown by the entropy perturbation $S' = S - S_0$ (–·–). The ordinates at unit amplitude are $U = 4.17$ E5, $T' = 2.94$ E3 and $S' = 1.98$ E7

Table 1. Shock heights in kilometers for different periods P and initial fluxes πF_I. Heights labeled e are obtained with the full hydrodynamic code; those labeled a are obtained with the method of Ulmschneider (1971b). Columns labeled S are values computed from Equation (6) of Stein and Schwartz (1972). Values are for an isothermal atmosphere of temperature $T = 4000$ K

	$\pi F_I = 2$ E7 erg/cm^2 s			$\pi F_I = 8$ E7 erg/cm^2 s		
P(s)	e	a	S	e	a	S
25	637	601	708	509	479	583
50	765	724	836	642	599	708
80	874	809	923	745	679	795

VII.2. Comparison with the Transform Method

One of us (Ulmschneider, 1971b) has given a simple method for the computation of acoustic waves in an arbitrary atmosphere. This method essentially transforms the shape of the velocity profile according to the requirements of energy conservation and simple wave theory; it becomes exact for zero gravity. Because this method is much faster on a computer and requires only a small fraction of the programing effort of the full hydrodynamic code, it is interesting to compare it with the present code. Table 1 shows the shock formation heights for different periods and initial fluxes in an isothermal gravitational atmosphere with $T_0 = 4000$ K and $g = 2.736$ E4 cm/s^2. The approximate method gives results with an error of about half a scale height. Considering the large range of fluxes and periods and the completely different approach, the agreement is good.

VII.3. The HSRA Atmosphere

Since the effects of radiative damping on acoustic waves depend on the radiative emission and absorption processes, it is desirable to compute as a first approximation the shock-formation heights in a solar model without radiative damping. Our model is the Harvard Smithsonian Reference Atmosphere (HSRA) (Gingerich et al., 1971). In order to show the situation in a radiative equilibrium atmosphere, this model was modified at heights above the temperature minimum according to the theoretical calculations of Kurucz (1974). The model, which is given in Table 1 of Paper III, is essentially the HSRA below 500 km. Figure 7 shows the height of shock formation as a function of period and initial flux. Here we have taken only periods that are near the range of calculated maximum acoustic power (Stein, 1968). The

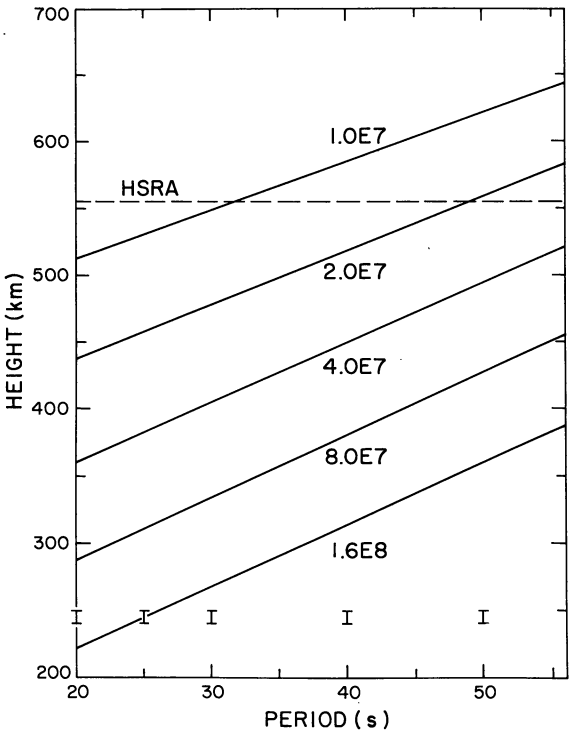

Fig. 7. Shock height (Euler variable) in the HSRA versus period. The initial flux of πF_I in erg/cm^2 s is indicated. Also shown is the location of the temperature minimum in the HSRA. Grid size is indicated by error bars

value of the flux is treated as a free parameter that is chosen in the range between 1 E7 to 2 E8 erg/cm^2 s. A flux of that magnitude is thought to be produced in the solar convection zone. It is seen that for a realistic acoustic flux the shock-formation height lies between 300 and 500 km. Only for the lowest fluxes and largest periods do shock heights occur that are above the empirical HSRA temperature minimum, as indicated in Figure 7. The shock height increases nearly linearly with period, in contrast to the isothermal cases. This behavior may be understood from the slowly decreasing temperature in the upper parts of the HSRA. As in the isothermal atmosphere, a decrease of the initial flux by a factor of two increases the height of shock formation by an almost constant height interval of about 70 km.

Acknowledgements. We are endebted to Drs. L. Cram, R. F. Stein and C. A. Whitney for reading the manuscript. This research was supported in part by NASA grant NGR 09-015-200. WK is grateful for the hospitality of Professor Hans Haffner, director of the Institut für Astrophysik of the University of Würzburg, and for the support of the German Academic Exchange Service (DAAD) during the summer of 1974.

References

Biermann, L.: 1946, *Naturwissenschaften* **33**, 118
Brezing, D.: 1965, *AIAA-J.* **3**, 1422
Cannon, C.J.: 1974, *J. Quant. Spectrosc. Radiat. Transfer* **14**, 761
Castor, J.I.: 1972, Dudley Observatory Reports **4**, A. G. D. Philip, Ed.
Courant, R., Friedrichs, K.O.: 1948, Supersonic Flow and Shock Waves, Interscience, New York
Gingerich, O., Noyes, R.W., Kalkofen, W., Cuny, Y.: 1971, *Solar Phys.* **18**, 347
Hartree, D.R.: 1952, Los Alamos Report LA-HU-1
Hines, C.O.: 1960, *Canadian J. Phys.* **38**, 1441
Hoskin, N.E.: 1964, *Meth. Comp. Phys.* **3**, 265
Kalkofen, W., Ulmschneider, P.: 1976, to be published
Klein, R.I.: 1973, Ph.D. Thesis, Brandeis University
Klein, R.I., Stein, R.F., Kalkofen, W.: 1976, *Astrophys. J.* **205**, 499
Kneer, F., Nakagawa, Y.: 1976, *Astron. Astrophys.* **47**, 65
Kurucz, R.: 1974, *Solar Phys.* **29**, 25
Landau, L.D., Lifshitz, E.M.: 1959, Fluid Mechanics, Pergamon Press, London
Leibacher, J.W.: 1971, Ph.D. Thesis, Harvard University
Lister, M.: 1960, in Math. Methods for Digital Computers I, Ralston, A., Wilf, H.S., eds., Wiley, New York
Pai, S.I.: 1966, Radiation Gas Dynamics, Springer-Verlag, New York
Pitteway, M.L.V., Hines, C.O.: 1965, *Canadian J. Phys.* **43**, 2222
Richardson, L.F., Gaunt, J.A.: 1927, *Trans. Roy. Soc. London* **226**, 300
Schwarzschild, M.: 1948, *Astrophys. J.* **107**, 1
Smith, R.R.: 1970, Ph.D. Thesis, University of California San Diego
Stefanik, R.: 1973, Ph.D. Thesis, Harvard University
Stein, R.F.: 1968, *Astrophys. J.* **154**, 297
Stein, R.F.: 1970, private communication
Stein, R.F.: 1972, private communication
Stein, R.F., Leibacher, J.W.: 1974, *Ann. Rev. Astron. Astrophys.* **12**, 407
Stein, R.F., Schwartz, R.A.: 1972, *Astrophys. J.* **177**, 807
Stein, R.F., Schwartz, R.A.: 1973, *Astrophys. J.* **186**, 1083
Ulmschneider, P.: 1970, *Astron. Astrophys.* **4**, 144
Ulmschneider, P.: 1971a, *Astron. Astrophys.* **12**, 297
Ulmschneider, P.: 1971b, *Astron. Astrophys.* **14**, 275
Ulmschneider, P.: 1974, *Solar Phys.* **39**, 327
Ulmschneider, P., Kalkofen, W.: 1976, to be published
Vincenti, W.G., Krüger, C.H.: 1965, Introduction to Physical Gas Dynamics, Wiley, New York
Zeldovich, Ya.B., Raizer, Yu.P.: 1967, Physics of Shock Waves and High-Temperature Hydrodynamic Phenomena, Academic Press, New York